Recent progress in piezo-phototronics with extended materials, application areas and understanding

Youfan Hu[1*] and Caofeng Pan[2] Zhong Lin Wang[2, 3]
[1]Key Laboratory for the Physics and Chemistry of Nanodevices, and Department of Electronics, Peking University, Beijing 100871, China
[2]Beijing Institute of Nanoenergy and Nanosystems, Chinese Academy of Sciences, Beijing 100083, China
[3]School of Material Science and Engineering, Georgia Institute of Technology, Atlanta, Georgia 30332-0245

*To whom correspondence should be addressed, E-mail: youfanhu@pku.edu.cn

Abstract

Coupling effect between different properties in a controllable manner is of great interesting for getting full understanding of materials, exploring novel physical phenomena and developing new applications. Piezo-phototronics is an emerging field which explores the three-way coupling among mechanical, optical and electrical properties in materials with noncentrosymmetric crystal structure. It has demonstrated its capability to work on different kinds of optoelectronic devices and be utilized in various applications. Here, we will give a briefly review on the tremendous progresses focusing on the extended materials, application areas and understanding in the last two years. New material systems including quantum wells, 2D materials and alloys were investigated in this field. Novel applications in sonophotocatalysis, flexible electronics, photoluminescence and plasmonics were emerged. Meanwhile, temperature dependence of piezo-phototronic effect was studied for the first time to get in-depth understanding of the fundamental physics behind the phenomena. All of these progresses demonstrate the power of this three-way coupling effect in extended fields and show the increasing broader interesting in different research areas.

1 Introduction

Since it was introduced in 2010[1, 2], the field of piezo-phototronics has attracted more and more research interest and gets very rapid development with great efforts in the past several years. It focuses on the three-way coupling of mechanical, optical and electrical properties in materials with noncentrosymmetric crystal structure. Previously it has been demonstrated that the strain induced localized polarization charges can effectively modulate/control the carrier generation, separation,

transport, and/or recombination by modifying the local electrical field distribution at the vicinity of metal-semiconductor (M-S) junction and homo-/hetero-junction. Different processes have been investigated to show the capability of the three-way coupling effect, including photodetection [3-8], photovoltaics [9-12], electroluminescence (EL) [13-17], photoelectrochemistry [19, 20], etc. Previous results demonstrated that, by optimizing built-in electric field to promote separation of photo-generated carriers, the sensitivity/responsibility of photodetector, the convention efficiency of solar cell and the performance of photoelectrochemical photoanodes can be enhanced greatly by piezo-phototronic effect. On the other hand, this effect can also be used to control EL properties via adjusted carrier injection efficiency or carrier recombination efficiency by modifying local electrical field at related interfaces. The controllable manner makes the piezo-phototronic effect versatile in various mechanical, optical and electrical coupled processes. As the understanding of the effect developed, and researchers with diverse background put their great efforts in, new material systems and novel application areas were emerged in the last two years. In this article, these progresses will be reviewed from three aspects. First we will focus on the progresses which utilize piezo-phototronic effect to optimize carrier generation and separation process, including the demonstrated enhancement of photoresponse in new material systems and applications in new areas. Then we move to the progress related to adjusting carrier recombination process, including the EL, photoluminescence (PL) and plasmonic effect associated new device platforms. Finally, the temperature dependence of piezo-phototronic effect is reviewed for further understanding of the fundamental physics. At the end, perspectives of this three-way coupling effect are presented.

2 Optimizing carrier generation and separation process

In general photoelectric process, electrons and holes generated under light illumination when the energy of the incident photons is equal or larger than the band gap of the semiconductor. Only the carriers that collected by electrodes are effective for photodetection or energy conversion in photovoltaic devices. Similarly in photoelectrochemical process, only the photoexcited carriers diffused onto the photoelectrode surface or photocatalyst surface can be used to perform electrochemical reduction reactions. Thus many approaches have been made to enhance the carrier separation efficiency in order to promote the performance of photodetectors/solar cells and the activity

of photocatalyst [21-26]. Previously piezo-phototronic effect has been demonstrated that it can take this responsibility to work on devices constructed with traditional piezoelectric material [3-12, 19, 20]. In the last two years, some new material combinations were investigated, such as ZnO/ ZnS core/shell nanowires [27, 28], Au-MgO-ZnO metal-insulator-semiconductor structure [29], $Mg_xZn_{1-x}O$/ Si p-n junction [30], ZnO/Spiro- MeOTAD heterojunction [31], etc. In the case of $Mg_xZn_{1-x}O$, ZnO thin film is alloyed with Mg to investigate how the alloying process and Mg content works on the piezoelectric coefficient and thus how the corresponding piezo-phototronic effect affects the performance improvement of photodetectors. Apart from these, new device platforms were introduced by utilizing this effect. Optical-fiber-ZnO/CdS nanowire hybridized structure was adapted to show the enhanced sensitivity and photoresponsivity in UV/ visible photosensing with piezo-phototronic effect [32]. In another case, asymmetric metal contacts were used on freestanding GaN membrane to construct metal-semiconductor-metal structure with enhanced on/off ration and sensitivity as a photoswitch by utilizing this effect [33]. However, the most interesting progress is the demonstration of piezo-phototronic effect on a single-atomic-layer MoS_2 [34].

In 2014, experimental results showed that thin MoS_2 flakes with an odd number of atomic layers had piezoelectric properties and a strong piezotronic effect was demonstrated in single-layer MoS_2 [35]. In the recent progress, the piezoelectric polarization charges created at the metal-MoS_2 interface are used to modulate the separation/transport of photogenerated carriers. In this work, mechanical exfoliated single-layer MoS_2 flakes were transferred onto a polyethylene terephthalate (PET) substrate, as shown in figure 1a. Cr/Pd/Au electrodes were deposited to make the metal-MoS_2 interface parallel to the "zigzag" direction of MoS_2. To investigate the piezo-phototronic process, a laser beam with a wavelength of 442 nm was illuminated on the device when strain was introduced in MoS_2 by bending substrate. Photocurrent was measured under systematically tuned optical illuminations and mechanical strains, as shown in figure 1b. It is clear that at a fixed strain condition photocurrent in MoS_2 increases as the illumination power density is increased. But if the illumination condition is fixed, the relationship between the photocurrent and the strain is not in such a monotonous form. Figure 1c shows three typical conditions. First, when there is no light illumination, the dark current in the device decreases with increasing compressive strain and increases with increasing tensile strain. While when laser illumination is on, maximum photocurrent is reached under different compressive strains for

different illumination intensities. To discuss the working mechanism, the result obtained under illumination intensity of 4.29 mW cm^{-2} is enlarged in figure 1d. Electron-hole pairs are generated under illumination in MoS_2. When there is no strain applied (1 in figure 1d), the built-in electric field at the Schottky contact area separates the electron and holes. The efficiency is limited and highly dependent on the barrier characteristics. When a mechanical strain is applied to the device (2-4 in figure 1d), induced piezoelectric polarization charges at the zigzag edges can affect the metal-MoS_2 contacts, which modify the Schottky barriers' height and width and thus tuning the optoelectronic process. There should be an optimized local electrical field distribution to get the highest electron-hole separation efficiency [36, 37], at which the highest photocurrent is obtained (3 in figure 1d). Under different illumination intensities, this situation is satisfied with different strain conditions. An optimized photoresponsivity of 2.3 $\times 10^4$ A W^{-1} is obtained in the flexible optoelectronics based on monolayer MoS_2, which is the highest number for monolayer MoS_2 phototransistors. This is the first demonstration of the piezo-phototronic effect on two-dimensional atomically thin materials. In another work, the photoresponsivity of a high performance MoS_2 field-effect transistor is enhanced by the piezo-phototronic effect via a bent GaN nanowire used as the local gate to introduce piezopotential for tuning [38]. These progresses may enable the development of flexible nanooptoelectromechanical systems, adaptive biooptoelectronic probes, and ultrathin optoelectronics.

Another important development should be mentioned individually is the emerging application in sonophotocatalysis [39]. Generally photoinduced carrier recombination in semiconductor photocatalyst is a big issue for low photocatalytic activity. Heterostructure can be used to introduce a built-in electric field in photocatalyst particles to promote photoinduced carrier separation [25, 26]. But a static field can be easily saturated by free carries in the space. Thus the enhancement of the photocatalysis will be vanished [40, 41]. In this work, Ag_2O-$BaTiO_3$ hybrid photocatalyst was synthesized as shown in figure 2a. Ag_2O nanoparticles (NPs) were assembled on $BaTiO_3$ nanocubes by chemical precipitation under ultrasonic irradiation. Ag_2O NPs work as the photocatalyst. There is a built-in electric field in ferroelectric $BaTiO_3$ nanocube because of its spontaneous polarization. This built-in field can be periodically altered through an ultrasonic wave utilizing the piezoelectric field generated in $BaTiO_3$ to avoid the saturation problem we mentioned above. The mechanism is illustrated in figure 2b. Therefore, enhanced carrier separation by the built-in field can be preserved

with the help of ultrasonic irradiation. Accordingly, the enhancement of photocatalytic performance of Ag_2O-$BaTiO_3$ hybrid photocatalyst can be maintained continuously. The photodegradation of Rh B under UV light irradiation with ultrasonic treatment was tested to compare the photocatalytic activity of Ag_2O and Ag_2O-$BaTiO_3$ hybrid nanostructure. Figure 2c and 2d are the absorption spectra of Rh B solution with different sonophotocatalysts. For Ag_2O, the sonophotocatalytic degradation rate of Rh B is only 90% in 2 h. However, for the Ag_2O−$BaTiO_3$ hybrid photocatalyst, the sonophotocatalytic degradation rate can reach 100% in the same time period. It shows that the utilization of piezo-phototronic effect will provide a new strategy for high performance photocatalysis applications.

3 Adjusting recombination process

Light-emitting diodes (LEDs) have attracted much scientific and commercial interest for the great application potential for artificial lighting and displays. Many approaches have been made to enhance the light emission intensity, which currently is a big obstacle toward the real application [42-46]. Carrier recombination is a very important step in EL related process. Previously demonstrated piezo-phototronic effect on controlling EL properties by adjusting carrier injection or recombination process is further proofed with different LED structures recently [47-49]. This three-way coupling among mechanical, optical and electrical properties also brings LED with new application in pressure mapping [16]. In the recent progress, this application has been extended into a flexible platform [50]. LED array composed of p-poly (3,4-ethylenedioxythiophene)- polystyrenesulfonate (PEDOT:PSS) and ZnO nanowires (NWs) was fabricated on a ITO/PET substrate. Figure 3a is an optical image of a fabricated flexible device. As shown in figure 3b, patterned ZnO NWS were first grown on the substrate. Then the inter-nanowire space was filled with SU8 to obtain good mechanical stability of the device. An Au film was deposited after spin-coating of PEDOT: PSS film to form a common top electrode with better conductivity. The pressure mapping performance was investigated by pressing a SU8 stamp with a convex character pattern of “BINN” on the device. Figure 3c shows the electroluminescence images of the device under pressure of 0, 22, 44, 66, and 88 MPa, respectively. Crosstalk between adjacent pixels is hardly observed. An enhancement factor E of the LED intensity is introduced to evaluate how pressure works on the change of light emission intensity. It is defined as $E=I_p/I_0$, where I_0 and I_p are the intensities of the LED under zero and corresponding pressures,

respectively. The relationship between enhancement factor and pressure of six devices is summarized in figure 3d. It shows a linear dependence. The change of emission light intensity obtained from six adjacent NW-LEDs under different pressures is recorded in figure 3e. It is clear that when the applied pressure increases the light emission intensity increases. The working mechanism is illustrated in figure 3f with the energy band diagram of the ZnO NW/p-polymer LED. The hole injection barrier at the interface is lowered under pressure which is induced by the inner-crystal piezo-potential. Therefore, the modified band structure increases the hole injection rate from PEDOT:PSS into ZnO and thus the recombination rate of carriers in ZnO NWs. This work also showed that the range of pressure measurement can be adjusted by varying the density and diameter of the ZnO NWs in each pixel via controlling the growth conditions of the ZnO NW arrays. It is very promising of such kind of devices to find its application in electronic skins.

For pressure mapping, researchers have also demonstrated another approach by utilizing photoluminescence imaging with piezo-phototronic effect for the first time [51]. In this work, InGaN/GaN multiple quantum well (MQW) pillar was realized by top-down fabrication from an epitaxial InGaN/GaN multilayer on a *c*-plane bipolished sapphire substrate, as shown in figure 4a. The density of the nanopillar array is 6.25×10^6 cm^{-2}. The diameter, height of each pillar, and distance between two adjacent pillars are 0.8, 1.2, and 4 μm, respectively. It corresponds to a pixel resolution of 6350 dpi. The uniformity is excellent. The inter-nanopillar space was filled with poly(methyl methacrylate) (PMMA), which is transparent in visible light range. Then the tips of the nanopillar array were exposed by oxygen plasma etching, as shown in figure 4b. PL image of the InGaN/GaN MQW nanopillar array was excited by a laser with a wavelength of 405 nm. Figure 4c is the recorded signal. It is very uniform in a large-area. Each pixel is a blue-light emitter, as shown in the insert of figure 4c. A good spatial resolution for pressure mapping is guaranteed by no cross-talk between adjacent blue-light spots. PL spectra of the MQW nanopillar array at different excitation power densities is shown in figure 4d. The PL intensity increased with increasing excitation optical power from 2 to 20 mW/mm^2. When pressure is applied to the structure, figure 4e presents the PL spectra recorded from a typical MQW nanopillar. It shows that the PL intensity have a very strong dependence on the magnitude of the applied pressure, while the PL peak wavelength is kept at the same. The relative PL intensity change ($|L_\sigma - L_0|/L_0$) as a function of applied pressure σ_s is presented in figure 4f, in which L_0 and L_σ denote the integral PL intensity between 420 and 513 nm under zero pressure

and the applied pressure introduced by a stamp with a convex character pattern of "BINN", respectively. For the nanopillar inside the stamp, it shows a linear relationship, while for the nanopillar outside the stamp, there is almost no response. This is because that the photogenerated electron-hole pairs in the MQW will be quickly separated by the increased built-in electric field under pressure, resulting in the decrease of radiative recombination probability and hence the increased PL intensity. Figure 4g is the optical image of the stamp with "BINN" character in contact with MQW nanopillar array. Figure 4h-j are the PL intensity differential images recorded under 1.87 MPa, 7.47 MPa and 14.94 MPa, respectively. High-resolution pressure image can be obtained by this approach. The advantage of this approach by utilizing PL is that it is all-optical method. The fabrication complexity will be reduced with no electrical interconnect layout required. It is suitable for large-area, highly uniform, and high-resolution sensing applications.

Plasmonic enhancement by metal NPs has offered new opportunities to engineer and improve the performance of optoelectronic device [52-55]. Recent work shows that localized surface plasmonic (LSP) resonance can be coupled with piezo-phototronic effect to enhance the PL of InGaN/GaN MQWs coated with Ag NPs [56]. The structure under investigation is schematically shown in figure 5a. InGaN/GaN MQW were grown on (0001)-oriented sapphire substrates by metal-organic chemical vapor deposition. The active region is composed of five-period $In_{0.17}Ga_{0.83}N$/GaN MQW structures with a thickness of 2.2 nm. Ag thin film was deposited on MQWs' top surface. Then Ag NPs with a mean size of 50 nm were obtained by annealing the sample at 300 °C for 5 min in N_2 atmosphere. MQWs-LSPs resonance process is schematically shown in figure 5b. In MQWs without coating, the photon-generated electron-hole pairs are terminated through radiative recombination k_{rad} or nonradiative recombinationk_{non}. When Ag NPs coating is introduced, electron-hole pairs excited within the MQW couple to electron vibrations at the metal/semiconductor interface when the energies of electron-hole pairs in MQW and of the metal LSP are similar. Then the resulting LSPs can be efficiently scattered as light as a result of inherent surface roughness in the evaporated metal coatings. This new recombination path increases the spontaneous recombination rate, and lead to the enhancement of light emission by LSP-MQW coupling [57]. To introduce piezo-phototronic effect, the sample is fixed by a jig on a plate, with a jackscrew pinning on the back to apply force at the center of the sample. Figure 5c shows the simulated tensile stress distribution when an external stress of 10 N is applied by using a finite-element analysis method. In order to facilitate direct comparison, Ag NPs

only covered half of the MQW's surface, and the other half is left bare. Figure 5d and 5e presents the PL spectrums of InGaN/GaN MQWs under straining condition without and with Ag NPs, respectively. The spectrums are measured on six equidistant points on the sample, as marked in figure 5c. Obviously, the PL intensity increases significantly from edge to the center with the increased stress and the peak wavelength gets blue shift in both cases. The shift of emission peak and integrated PL intensity with different recording locations of the two cases is plotted in figure 5f and 5g, respectively. The increasing magnitude of PL intensity is larger for Ag NPs-coated MQWs than the bared MQWs. The theoretical calculation indicated that the spatial overlap of electron-heavy hole and electron- light hole both increase with external strains and so does the effective bandgap, as shown in figure 5h. Thus the blue shift of PL peak ascribed to increased effective bandgap with reduced piezoelectric field, while the monotonous increase of PL intensity is attributed to the piezo-phototronic effect. This research provides an approach to utilizing plasmonics with piezo-phototronic effect and brings widespread applications of piezo-phototronics to high-efficiency artificial lighting, on-chip integrated plasmonic circuits, etc.

4 Understanding the physics of piezo-phototronic effect

Temperature dependence behavior is very meaningful for understanding the physics of a property or phenomenon [58-61]. Previously temperature dependence of piezotronic effect has been investigated for proofing the proposed fundamental mechanism [62]. Recently, the temperature dependence of the three-way coupling among mechanical, optical and electrical properties in cadmium sulfide nanowires (CdS NWs) is systematically investigated by varying the temperature from 77 to 300 K, and the piezo-phototronic effect is significantly enhanced by over 550% as lowering the system temperature [63]. In this work, CdS NW devices were fabricated on aluminum foil covered with a layer of Kapton tape. The electric properties of the device were measured in a micromanipulation cryogenic probe system, as shown in the insert of figure 6a. The device can be bent with the micromanipulator and a beam of green laser (wavelength = 532 nm) was introduced to shin on the device. Figure 6a is the typical I-V characteristic to show the temperature dependence of the devices under illumination. When there is no strain, the current passing through the device decreases as the system temperature decreases under an optical illumination density of 1.58 mW cm^{-2}. At 77 k with the same illumination condition,

when strain is introduced, the output currents increase at positive biased voltages while decrease at the negative side when the externally applied tensile strains are increased, as shown in figure 6b. A physical parameter, piezo-phototronic factor, is defined as the response sensitivity per unit strain:

$$\frac{S}{d\varepsilon} = \frac{I_{\varepsilon_2} - I_{\varepsilon_1}}{I_{\varepsilon_1}(\varepsilon_2 - \varepsilon_1)}$$

where I_{ε_2} and I_{ε_1} correspond to the photocurrent under ε_2 and ε_1 straining conditions at the same illumination intensity, respectively. The piezo-phototronic factors under -4 and +5 V biased voltages are plotted as a function of temperatures with different illumination intensities in figure 6c and 6d, respectively. A larger piezo-phototronic factor is observed at lower temperature for all the cases. To further understanding this phenomenon, changes of Schottky barrier height (SBH) are simulated by a program PKUMSM based on an M-S-M model [64]. The calculated changes of SBH as a function of temperature at the reversely biased Schottky contact under -4 and +5 V bias voltages are shown in figure 6e and 6f, respectively. The significantly enhanced piezo-phototronic effect at low temperatures is attributed to the effective polarization charges increase, which leads to more changes in the SBH. It results from the reduced screening effect caused by the decreased charge carriers mobility and density when the system is cooling down. In another work, temperature dependence of piezo-phototronic effect in *a*-axis GaN nanobelts was investigated [65]. In this material system, there is a competition between the enhanced attraction of electrons to noncompletely screened positive piezocharges and the enhanced detrapping/activation of bounded electrons, which leads to a local minimum of output currents at certain straining condition. Both of these works investigate the temperature dependence and the fundamental working mechanism of the piezo-phototronic effect, providing guidance for the design and fabrication of piezo-phototronic optoelectronic devices.

5 Perspectives

Piezo-phototronics provide a new platform for materials research and new optoelectronic device explorations. The three-way coupling essence makes this area attractive for all researchers from mechanical, optical and electrical background. And also this essence means that its development needs multidisciplinary contributions. The rapid progress of piezo-phototronics in the last several years has proved this. The controllable tuning characteristics make it very powerful to introduce new vitality to

traditional devices and explore devices with new working principle. The extended material systems, emerging application areas and further understanding of piezo-phototronics we reviewed here is just a short summary of the recent progress in the last two years. More things are waiting to explore to further release the huge potential of piezo-phototronics. The boom of this field is expected.

Acknowledgment

This work was supported by the National Science Foundation of China (Grant No. 61571016), "Thousand Talents" Program for the pioneer researchers, the National Key Research & Development Program (Grant No. 2016YFA0201901), and the Foundation for Innovative Research Groups of the National Natural Science Foundation of China (Grant No. 61621061).

Reference:

[1] Hu Y F, Chang Y L, Fei P, Snyder R L and Wang Z L 2010 Designing the electric transport characteristics of ZnO micro/nanowire devices by coupling piezoelectric and photoexcitation effects *ACS Nano* **4**, 1234-40.

[2] Wang Z L 2010 Piezopotential gated nanowire devices: Piezotronics and piezo-phototronics *Nano Today* **5**, 540-52.

[3] Yang Q, Guo X, Wang W H, Zhang Y, Xu S, Lien D H and Wang Z L 2010 Enhancing sensitivity of a single ZnO micro-/nanowire photodetector by piezo-phototronic effect *ACS Nano* **4**, 6285-91.

[4] Zhang F, Ding Y, Zhang Y, Zhang X L and Wang Z L 2012 Piezo-phototronic effect enhanced visible and ultraviolet photodetection using a ZnO/CdS core/shell micro/nanowire *ACS Nano* **6**, 9229-36.

[5] Dong L, Niu S M, Pan C F, Yu R M, Zhang Y and Wang Z L 2012 Piezo-phototronic effect of CdSe nanowires *Adv. Mater.* **24**, 5470-5.

[6] Zhang F, Niu S M, Guo W X, Zhu G, Liu Y, Zhang X L and Wang Z L 2013 Piezo-phototronic effect enhanced visible/UV photodetector of a carbon-fiber/ZnO-CdS double-shell microwire *ACS Nano* **7**, 4537-44.

[7] Wang Z N, Yu R M, Wen X N, Liu Y, Pan C F, Wu W Z and Wang Z L 2014 Optimizing performance of silicon- based p-n junction photodetectors by the piezo-phototronic effect *ACS Nano* **8**, 12866-73.

[8] Zhang Z, Liao Q L, Yu Y H, Wang X D and Zhang Y 2014 Enhanced photoresponse of ZnO nanorods-based self-powered photodetector by piezotronic interface engineering *Nano Energy* **9**, 237-44.

[9] Hu Y F, Zhang Y, Chang Y L, Snyder R L and Wang Z L 2010 Optimizing the power output of a ZnO photocell by piezopotential *ACS Nano* **4**, 4220-4.

[10] Pan C F, Niu S M, Ding Y, Dong L, Yu R M, Liu Y, Zhu G and Wang Z L 2012 Enhanced Cu_2S/CdS coaxial nanowire solar cells by piezo- phototronic effect *Nano Lett.* **12**, 3302-7.

[11] Wen X N, Wu W Z and Wang Z L 2013 Effective piezo-phototronic enhancement of solar cell performance by tuning material properties *Nano Energy* **2**, 1093-110.

[12] Shi J, Zhao P and Wang X D 2013 Piezoelectric-polarization-enhanced photovoltaic performance in depleted-heterojunction quantum-dot solar cells *Adv. Mater.* **25**, 916-21.

[13] Yang Q, Wang W H, Xu S and Wang Z L 2011 Enhancing light emission of ZnO microwire-based diodes by piezo-phototronic effect *Nano Lett.* **11**, 4012-7.

[14] Hu Y F, Zhang Y, Lin L, Ding Y, Zhu G and Wang Z L 2012 Piezo-phototronic effect on electroluminescence properties of p- type GaN thin films *Nano Lett.* **12**, 3851-6.

[15] Zhang Y, Gao G, Chan H L W, Dai J Y, Wang Y and Hao J H 2012 *Adv. Mater.* 24, 1729.

[16] Pan C F, Dong L, Zhu G, Niu S M, Yu R M, Yang Q, Liu Y and Wang Z L 2013 High-resolution electroluminescent imaging of pressure distribution using a piezoelectric nanowire LED array *Nature Photon.* **7**, 752-8.

[17] Bai G X, Zhang Y and Hao J H 2014 Tuning of near-infrared luminescence of $SrTiO_3$:Ni^{2+} thin films grown on piezoelectric PMN-PT via strain engineering *Sci. Rep.* **4**, 5724.

[18] Wang C F, Bao R R, Zhao K, Zhang T P, Dong L and Pan C F 2014 Enhanced emission intensity of vertical aligned flexible ZnO nanowire/p-polymer hybridized LED array by piezo-phototronic effect *Nano Energy* **14**, 364-71.

[19] Shi J, Starr M B, Xiang H, Hara Y, Anderson M A, Seo J-H, Ma Z Q and Wang X D 2011 Interface engineering by piezoelectric potential in ZnO-based photoelectrochemical anode *Nano Lett.* **11**, 5587-93.

[20] Li H X, Yu Y H, Starr M B, Li Z D and Wang X D 2015 Piezotronic-enhanced photoelectrochemical reactions in $Ni(OH)_2$-decorated ZnO photoanodes *J. Phys. Chem. Lett.* **6**, 3410-6.

[21] Cho N, Choudhury K R, Thapa R B, Sahoo Y, Ohulchanskyy T, Cartwright A N, Lee K-S and Prasad P N 2007 Efficient photodetection at IR wavelengths by incorporation of PbSe–carbon-nanotube conjugates in a polymeric nanocomposite *Adv. Mater.* **19**, 232-6.

[22] Tian B Z, Kempa T J and Lieber C M 2009 Single nanowire photovoltaics *Chem. Soc. Rev.* **38**, 16-24.

[23] Brabec C J, Sariciftci N S and Hummelen J C 2001 Plastic solar cells *Adv. Funct. Mater.* **11**, 15-26.

[24] Yu G, Gao J, Hummelen J C, Wudl F and Heeger A J 1995 Polymer photovoltaic cells: enhanced efficiencies via a network of internal donor-acceptor heterojunctions *Science* **270**, 1789-91.

[25] Abdi F F, Han L H, Smets A H M, Zeman M, Dam B and Krol R V D 2013 Efficient solar water splitting by enhanced charge separation in a bismuth vanadate-silicon tandem photoelectrode *Nature Commun.* **4**, 2195.

[26] Marschall R 2014 Semiconductor composites: strategies for enhancing charge carrier separation to improve photocatalytic activity *Adv. Funct. Mater.* **24**, 2421-40.

[27] Rai S C, Wang K, Ding Y, Marmon J K, Bhatt M, Zhang Y, Zhou W L and Wang Z L 2015 Piezo-phototronic effect enhanced UV/visible photodetector based on fully wide band gap type-II ZnO/ZnS core/shell nanowire array *ACS Nano* **9**, 6419-27.

[28] Jeong S, Kim M W, Jo Y-R, Leem Y-C, Hong W-K, Kim B-J and Park S-J, 2016 High-performance photoresponsivity and electrical transport of laterally grown ZnO/ZnS core/shell nanowires by the piezotronic and piezophototronic effect *Nano Energy* **30**, 208-16.

[29] Liao Q L, Liang M Y, Zhang Z, Zhang G J and Zhang Y 2015Strain-modulation and service behavior of Au–MgO–ZnO ultraviolet photodetector by piezo-phototronic effect *Nano Res.* **8**, 3772-9.

[30] Chen Y-Y, Wang C-H, Chen G-S, Li Y-C and Liu C-P 2015 Self-powered n-$Mg_xZn_{1-x}O$/p-Si photodetector improved by alloying-enhanced piezopotential through piezo-phototronic effect *Nano Energy* **11**, 533-9.

[31] Shen Y W, Yan X Q, Si H N, Liu Y C, Sun Y H and Zhang Y 2016 Improved photoresponse performance of self-powered ZnO/Spiro- MeOTAD heterojunction ultraviolet photodetector by piezo- phototronic effect *ACS Appl. Mater. Interfaces* **8**, 6137-43.

[32] Wang Z N, Yu R M, Pan C F, Liu Y, Ding Y and Wang Z L 2015 Piezo-phototronic UV/visible photosensing with optical-fiber–nanowire hybridized structures *Adv. Mater.* **27**, 1553-60.

[33] Peng M Z, Liu Y D, Yu A F, Zhang Y, Liu C H, Liu J Y, Wu W, Zhang K, Shi X Q, Kou J Z, Zhai J Y and Wang Z L 2016 Flexible self-powered GaN ultraviolet photoswitch with piezo-phototronic effect enhanced on/off ratio *ACS Nano***10**, 1572-9.

[34] Wu W Z, Wang L, Yu R M, Liu Y Y, Wei S-H, Hone J and Wang Z L 2016 Piezophototronic effect in single-atomic-layer MoS_2 for strain-gated flexible optoelectronics *Adv. Mater.* **28**, 8463-8.

[35] Wu W Z, Wang L, Li Y L, Zhang F, Lin L, Niu S M, Chenet D, Zhang X, Hao Y F, Heinz T F, Hone J and Wang Z L 2014 Piezoelectricity of single-atomic-layer MoS_2 for energy conversion and piezotronics *Nature* **514**, 470-4.

[36] Liu Y, Yang Q, Zhang Y, Yang Z Y and Wang Z L 2012 Nanowire piezo-phototronic photodetector: theory and experimental design *Adv. Mater.* **24**, 1410-7.

[37] Liu Y, Zhang Y, Yang Q, Niu S M and Wang Z L 2015 Fundamental theories of piezotronics and piezo-phototronics *Nano Energy* **14**, 257-75.

[38] Liu X Q, Yang X N, Gao G Y, Yang Z Y, Liu H T, Li Q, Lou Z, Shen G Z, Liao L, Pan C F and Wang Z L 2016 Enhancing photoresponsivity of self-aligned MoS_2 field-effect transistors by piezo-phototronic effect from GaN Nanowires *ACS Nano* **10**, 7451-7.

[39] Li H D, Sang Y H, Chang S J, Huang X, Zhang Y, Yang R S, Jiang H D, Liu H and Wang Z L 2015 Enhanced ferroelectric-nanocrystal-Based hybrid photocatalysis by ultrasonic-wave-generated piezophototronic effect *Nano Lett.* **15**, 2372-9.

[40] Tiwari D and Dunn S 2009 Photochemistry on a polarisable semi-conductor: what do we understand today? *J. Mater. Sci.* **44**, 5063−79.

[41] Li L, Salvador P A and Rohrer G S 2014 Photocatalysts with internal electric fields *Nanoscale* **6**, 24-42

[42] Erchak A A, Ripin D J, Fan S H, Rakich P, Joannopoulos J D, Ippen E P, Petrich G S and Kolodziejski L A 2001 Enhanced coupling to vertical radiation using a two-dimensional photonic crystal in a semiconductor light-emitting diode *Appl. Phys. Lett.* **78**, 563.

[43] Huh C, Lee K-S, Kang E-J and Park S-J 2003 Improved light-output and electrical performance of InGaN-based light-emitting diode by microroughening of the p-GaN surface *J. Appl. Phys.* **93**, 9383.

[44] Kim D-H, Cho C-O, Roh Y-G, Jeon H, Park Y S, Cho J, Im J S, Sone C, Park Y, Choi W J, and Park Q-H 2005 Enhanced light extraction from GaN-based light-emitting diodes with holographically generated two-dimensional photonic crystal patterns *Appl. Phys. Lett.* **87**, 203508.

[45] Zhong J, Chen H, Saraf G, Lu Y, Choi C K, Song J J, Mackie D M and Shen H 2007 Integrated ZnO nanotips on GaN light emitting diodes for enhanced emission efficiency *Appl. Phys. Lett.* **90**, 203515.

[46] Kwon M-K, Kim J-Y, Kim B-H, Park I-K, Cho C-Y, Byeon C C and Park S-J 2008 Surface-plasmon-enhanced light-emitting diodes *Adv. Mater.* **20**, 1253-7.

[47] Guo Z, Li H W, Zhou L Q, Zhao D X, Wu Y H, Zhang Z Q, Zhang W, Li C Y and Yao J 2015 Large-scale horizontally aligned ZnO microrod arrays with controlled orientation, periodic distribution as building blocks for chip-in piezo-phototronic LEDs *Small*, **11**, 438-45.

[48] Kim K, Jeon Y, Cho K and Kim S 2016 Enhancement of trap-assisted green electroluminescence efficiency in ZnO / SiO_2 / Si nanowire light-emitting diodes on bendable substrates by piezophototronic effect *ACS Appl. Mater. Interfaces* **8**, 2764-73.

[49] Chen M X, Pan C F, Zhang T P, Li X Y, Liang R R and Wang Z L 2016 Tuning light emission of a pressure-sensitive silicon/ZnO nanowires heterostructure matrix through piezo-phototronic effects *ACS Nano* **10**, 6074-9.

[50] Bao R R, Wang C F, Dong L, Yu R M, Zhao K, Wang Z L and Pan C F 2015 Flexible and controllable piezo-phototronic pressure mapping sensor matrix by ZnO NW/p-polymer LED array *Adv. Funct. Mater.* **25**, 2884-91.

[51] Peng M Z, Li Z, Liu C H, Shi X Q, Song M, Zhang Y, Du S Y, Zhai J Y and Wang Z L 2015 High-resolution dynamic pressure sensor array based on piezo-phototronic effect tuned photoluminescence imaging *ACS Nano* **9**, 3143-50.

[52] Stewart M E, Anderton C R, Thompson L B, Maria J, Gray S K, Rogers J A and Nuzzo R G 2008 Nanostructured plasmonic sensors *Chem. Rev.* **108**, 494-521.

[53] Jiang R B, Li B X, Fang C H and Wang J F 2014 Metal/semiconductor hybrid nanostructures for plasmon-enhanced applications *Adv. Mater.* **26**, 5274-309.

[54] Liang Z Q, Sun J, Jiang Y Y and Chen X D 2014 Plasmonic enhanced optoelectronic devices *Plasmonics* **9**, 1-8.

[55] Li M, Cushing S K and Wu N Q 2015 Plasmon-enhanced optical sensors: a review *Analyst* **140**, 386-406.

[56] Huang X, Jiang C Y, Du C H, Jing L, Liu M M, Hu W G and Wang Z L 2016 Enhanced luminescence performance of quantum wells by coupling piezo-phototronic with plasmonic effects *ACS Nano* **10**, 11420-7.

[57] Okamoto K, Niki I, Shvartser A, Narukawa Y, Mukai T and Scherer A 2004 Surface-plasmon-enhanced light emitters based on InGaN quantum wells *Nature Mater.* **3**, 601-5.

[58] Bosman A J and Havinga E E 1963 Temperature dependence of dielectric constants of cubic ionic compounds *Phys. Rev.* **129**, 1593

[59] Varshni Y P 1967 Temperature dependence of the energy gap in semiconductors *Physica* **34**, 149-54.

[60] Fernandez C D J 2005 Influence of the temperature dependence of anisotropy on the magnetic behavior of nanoparticles *Phys. Rev. B* **72**, 054438.

[61] Sjostrom T, Harris F E and Trickey S B 2012 Temperature-dependent behavior of confined many-electron systems in the Hartree-Fock approximation *Phys. Rev. B* **85**, 045125.

[62] Hu Y F, Klein B D B, Su Y J, Niu S M, Liu Y and Wang Z L 2013 Temperature dependence of the piezotronic effect in ZnO nanowires *Nano Lett.* **13**, 5026-32.

[63] Yu R M, Wang X F, Wu W Z, Pan C F, Bando Y, Fukata N, Hu Y F, Peng W B, Ding Y and Wang Z L 2015 Temperature dependence of the piezophototronic effect in CdS nanowires *Adv. Funct. Mater.* **25**, 5277-84.

[64] Liu Y, Zhang Z Y, Hu Y F, Jin C H and Peng L M 2008 Quantitative fitting of nonlinear current-voltage curves and parameter retrieval of semiconducting nanowire, nanotube and nanoribbon devices *J. Nanosci. Nanotechnol.* **8**, 252-8.

[65] Wang X F, Yu R M, Peng M Z, Wu W Z, Li S T and Wang Z L 2015 Temperature dependence of the piezotronic and piezophototronic effects in a-axis GaN nanobelts *Adv. Mater.* **27**, 8067-74.

Figures

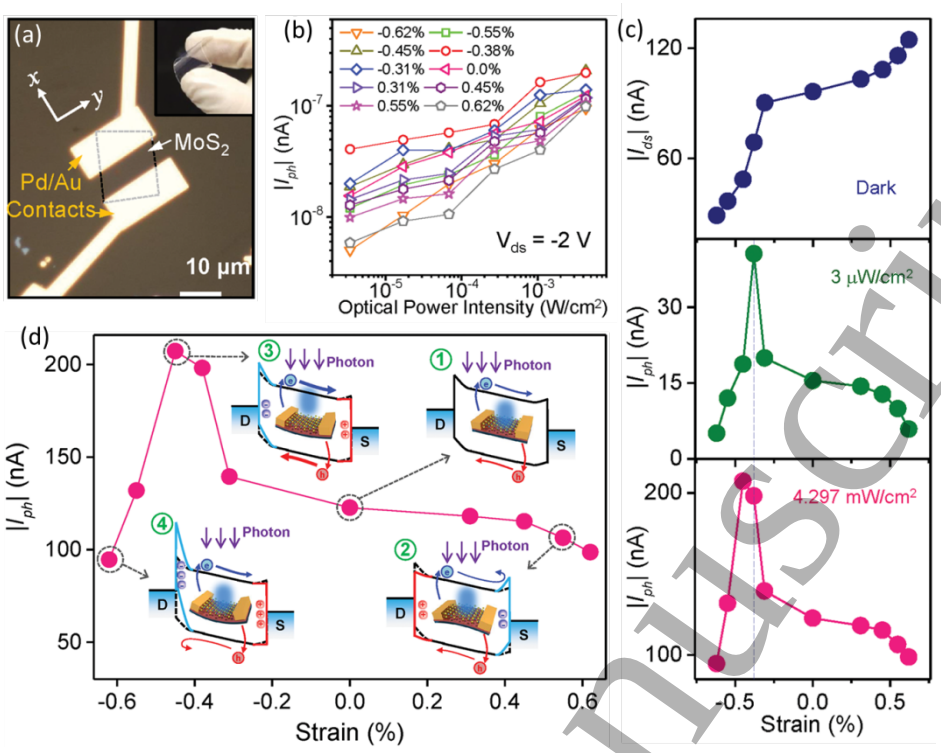

Figure 1 (a) Optical image of flexible phototransistor constructed with monolayer MoS_2 on PET substrate. The insert shows the flexibility of the device. (b) Change in photocurrent by strain under different illumination intensities. (c) Strain dependence of the dark current (top) and photocurrent (middle and bottom). (d) Working mechanism of piezo-phototronic response in single layer MoS_2 phototransistor. Reproduced with permission from reference [34].

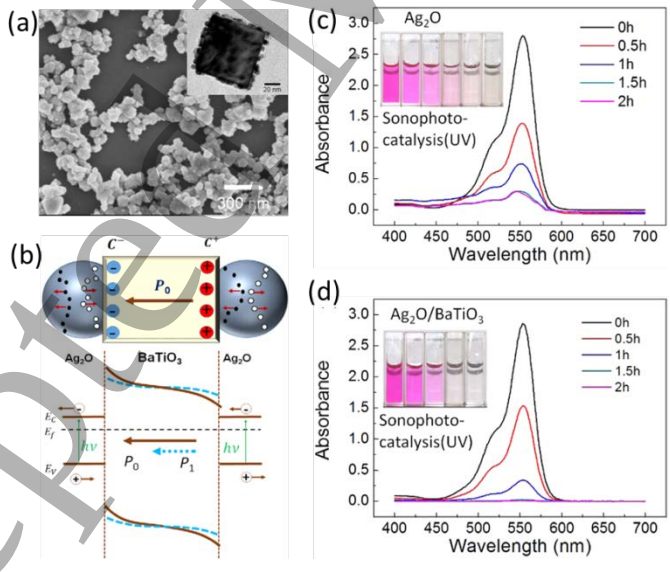

Figure 2 (a) SEM images of Ag_2O-$BaTiO_3$ hybrid nanocubes, the insert is a TEM image. (b) Working mechanism of the piezo-phototronic effect on sonophotocatalysis of the hybrid structure. (c) The absorption spectra of Rh B solution with Ag_2O under UV light irradiation with ultrasonic treatment. (d) The absorption spectra of Rh B solution with Ag_2O-$BaTiO_3$ hybrid nanocubes under UV light irradiation with ultrasonic treatment. Reproduced with permission from reference [39].

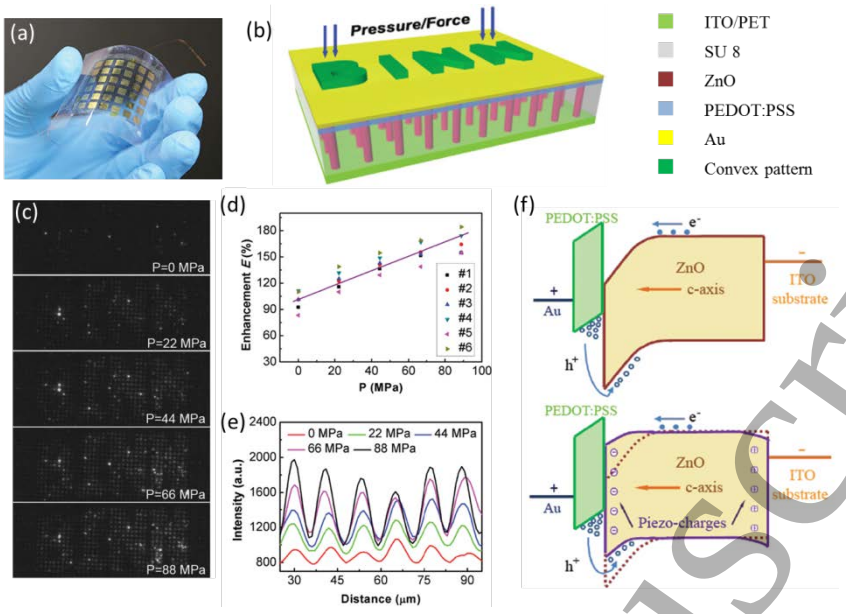

Figure 3 (a) Optical image of a fabricated flexible device with LED arrays for pressure mapping. (b) Schematic illustration of the NW-LED-based pressure sensor arrays. (c) EL images of the device under pressure of 0, 22, 44, 66, and 88 MPa, respectively. (d) Enhancement factor *E* of six NW-LEDs as a function of applied compressive pressure of up to 88 MPa. (e) The change of emission light intensity obtained from six adjacent NW-LEDs under different pressures. (f) Schematic band diagram of an n-ZnO/p-polymer p-n junction without (top) and with (solid line in the bottom) applied compressive strain. Reproduced with permission from reference [50].

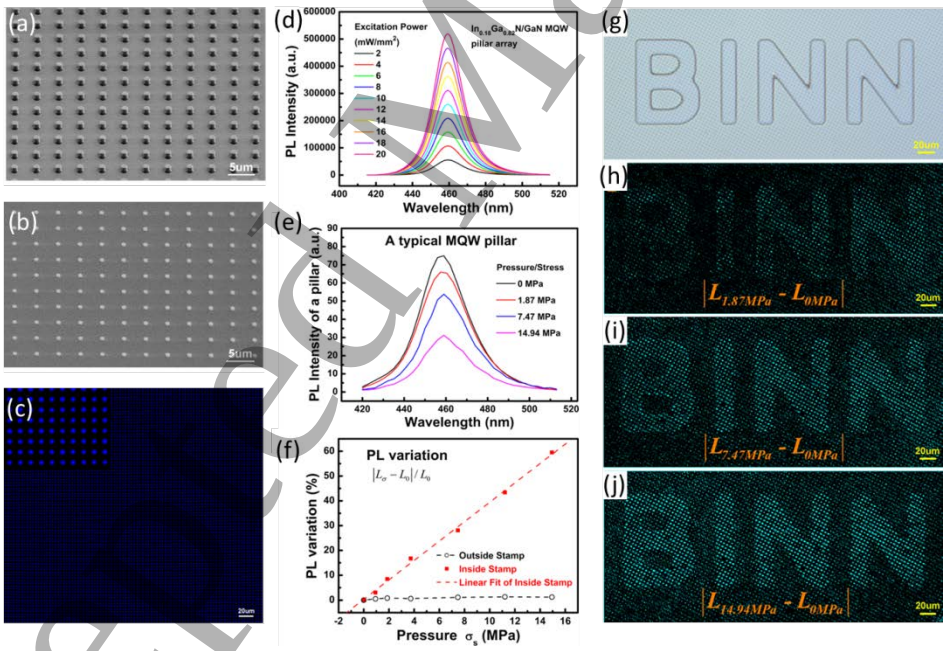

Figure 4 (a) SEM image of InGaN/GaN MQW nanopillar (b) SEM image of the pillar array after PMMA coating and oxygen plasma etching to expose tips. (c) PL image of MQW pillar array. (d) PL spectra of the MQW pillar array at different excitation power densities. (e) PL spectra of a typical MQW pillar under different pressure. (f) Changes of PL intensity inside and outside the BINN stamp as a function of the applied pressure. (g) Optical image of the BINN stamp in contact with the MQW nanopillar array (h-j) PL intensity differential images recorded under 1.87 MPa, 7.47 MPa and 14.94 MPa, respectively. Reproduced with permission from reference [51].

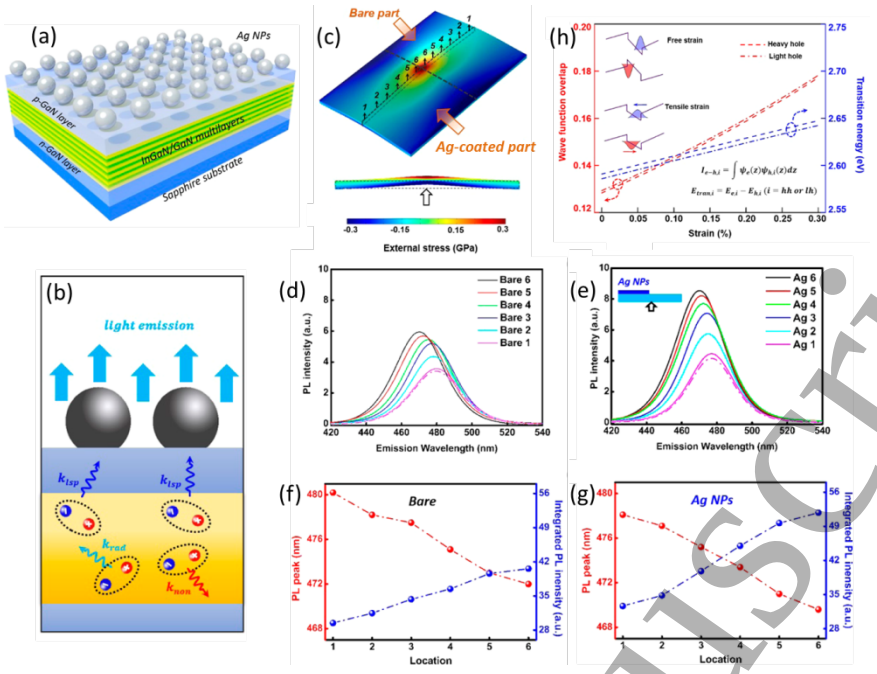

Figure 5 (a) Schematic view of Ag NPs-coated InGaN/GaN MQWs. (b) Schematic diagram to show the mechanism of LSP-MQWs resonance process. (c) Simulated distribution of tensile stress induced by an external applied stress of 10 N. PL performance under straining condition for (d) bare InGaN/GaN MQWs, and (e) Ag NPs coated InGaN/GaN MQWs. The shift of PL emission peak and integrated PL intensity for (f) bare InGaN/GaN MQWs, and (g) Ag NPs-coated MQWs. Reproduced with permission from reference [56].

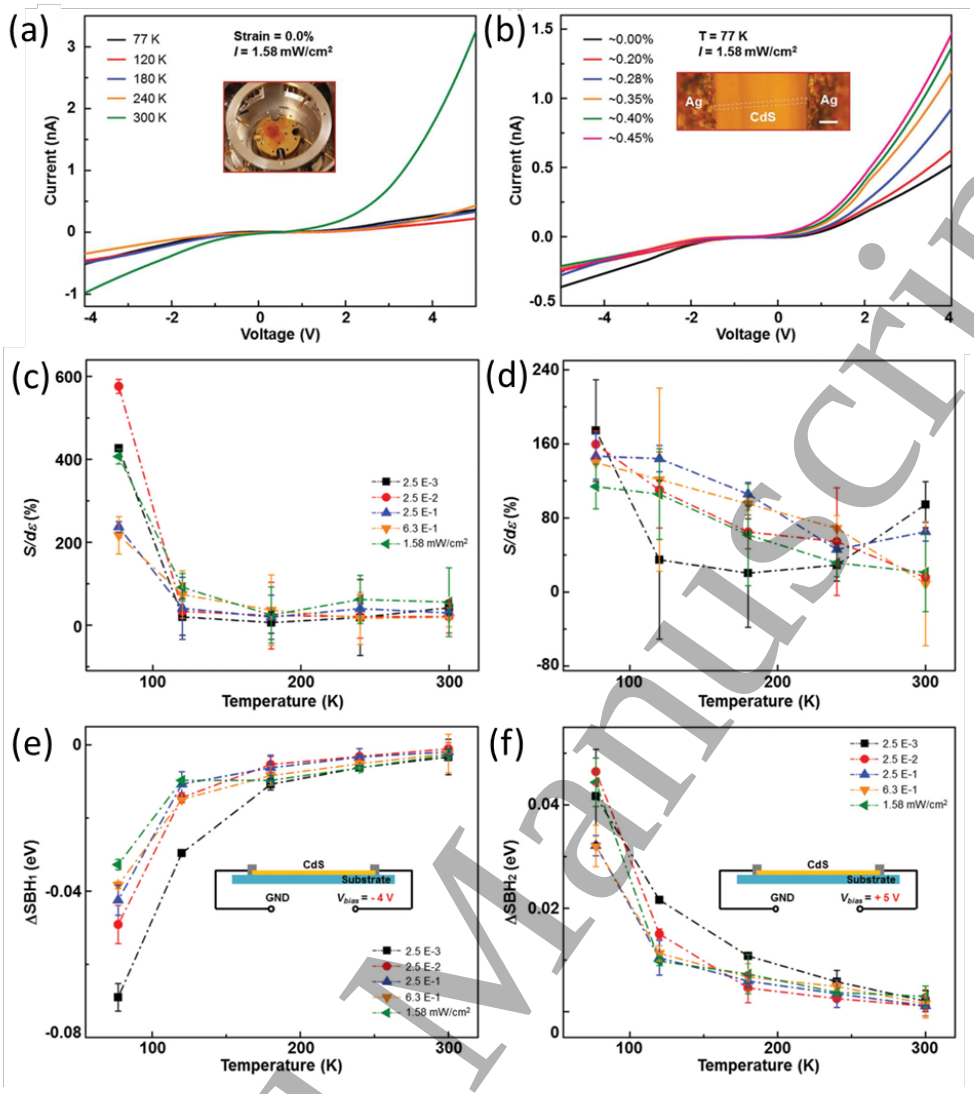

Figure 6 (a) Typical I-V characteristic of CdS NW device at various temperatures under illumination. (b) Typical I-V characteristic of CdS NW devices at 77 K with applied strain under illumination. The piezo-phototronic factors as a function of temperatures with different illumination intensities under (c) -4 and (d) +5 V biased voltages. Calculated changes of SBH as a function of temperature at the reversely biased Schottky contact under (e) -4 and (f) +5 V biased voltages. Reproduced with permission from reference [63].